J. Plasma Physics (2007), *vol.* 73, *part* 4, *pp.* 575–589. © 2006 Cambridge University Press
doi:10.1017/S0022377806004867 First published online 6 September 2006 Printed in the United Kingdom

Dust voids (holes) in a charge-varying complex plasma with non-isothermal trapped electrons

MOULOUD TRIBECHE, LEILA AIT GOUGAM, SAFIA GRIBA and TAHA HOUSSINE ZERGUINI

Faculty of Sciences-Physics, Theoretical Physics Laboratory, Plasma Physics Group, University of Bab-Ezzouar, USTHB, B.P. 32, El Alia, Algiers 16111, Algeria

(Received 16 May 2006)

Abstract. The recent analysis of dust voids (Mamun, A. A. and Shukla, P. K. 2005 *J. Plasma Phys.* **71**, 143) is extended to include self-consistent electron trapping and dust charge variation. It is found that under certain conditions the effect of dust charge variation can be quite important. In particular, it may be noted that the dust charge variation leads to an additional enlargement of the nonlinear dust voids. The effects of ion/electron temperature and trapping parameter on the properties of these nonlinear dust voids are briefly discussed. As the dust particle number density is increased, the depth, as well as the width, of the dust void decreases and the additional enlargement (due to dust charge perturbations) becomes less pronounced. Furthermore, these dust voids exhibit smaller widths than those involving isothermal electrons.

1. Introduction

Recently, there has been a rapidly growing interest in the study of different types of collective processes in dusty plasmas, because of their relevance and vital role in laboratory, space, and astrophysical plasma environments, such as cometary tails, asteroid zones, planetary rings, interstellar medium, the Earth's ionosphere, and magnetosphere, etc. [1–5]. In addition, dust particles have been observed in low-temperature plasmas, similar to those used in plasma processing and plasma crystals. It has been shown both theoretically and experimentally that the presence of these extremely massive and highly charged dust grains in a plasma can modify the behavior of the usual waves and instabilities, and that their dynamics introduces new eigenmodes [6–10]. The most well studied of such modes is the so-called dust-acoustic mode [6], which arises due to the restoring force provided by the plasma thermal pressure (electrons and ions) while the inertia is due to the dust mass.

Recently, a number of experiments in dusty plasmas have shown the formation and existence of stable dust-free regions (voids) with sharp boundaries inside a dust cloud. These voids have been observed both in laboratory experiments and under microgravity conditions, and a number of theoretical models have been proposed to explain the physics of their formation [11–31].

Recently, Mamun and Shukla [32] proposed a theoretical model to explain the physics of the void formation. It was shown that a dust void can be formed due

https://doi.org/10.1017/S0022377806004867 Published online by Cambridge University Press

to the presence of a positive plasma potential, which is built up due to a non-isothermal dust particle distribution arising from negatively charged dust particle trapping. The aim of the present paper is therefore to extend the analysis of Mamun and Shukla [32], performed under the assumption that the charge on the dust grains remains constant, to include self-consistent charge variations and electron trapping. The outline of the paper is as follows. In the next section, we present the basic equations of the model. The results are presented and discussed in Sec. 3. A summary of our results and conclusions is given in Sec. 4.

2. Theoretical model

We consider an unmagnetized dusty plasma having electrons, positive ions, and dust grains of density n_e, n_i, and n_d, respectively. We assume for simplicity that all the grains have the same charge, equal to $q_d = -eZ$, with Z positive for negatively charged dust grains and negative for positively charged dust grains. All the dust grains are assumed to be of the same size and to be spheres of radius r. The ions are assumed to be in thermal equilibrium, with the density given by

$$n_i = n_{i0} \exp\left(-\frac{e\phi}{T_i}\right). \tag{1}$$

To model the hot electron distribution in the presence of trapped particles, we employ a vortex-like electron distribution function of Schamel [33–36]. Thus, we have

$$n_e = n_{e0}\left\{\exp\left(\frac{e\phi}{T_{ef}}\right)\mathrm{erfc}\left(\sqrt{\frac{e\phi}{T_{ef}}}\right) + \frac{2}{\sqrt{-\pi\beta_e}} W\left(\sqrt{-\beta_e \frac{e\phi}{T_{ef}}}\right)\right\}, \tag{2}$$

where $j = e, i$ denote electrons and ions, respectively, ϕ is the electrostatic potential, $q_{j=e,i} = \mp e$ are the charges, and T_j the temperatures. The subscript 0 stands for equilibrium values and f (t) represents the free (trapped) electron contribution. Here β_e is a parameter determining the number of trapped electrons and its magnitude is defined as the ratio of the free hot-electron temperature T_{ef} to the hot trapped electron temperature T_{et}, i.e. $|\beta_e| = T_{ef}/T_{et}$. $W(x)$ is the Dawson integral, namely $W(x) = \exp(-x^2)\int_0^x \exp(t^2)\,dt$.

The variable charge dust particles are described by the coupled set of Vlasov–Poisson equations, which we solve by using the second procedure as given in [33–36]. Accordingly, in order to solve the Vlasov equation for dust particles with variable charge, we make use of an appropriate ansatz in terms of the constants of motion. To model the hot dust distribution in the presence of trapped particles, we refer to an appropriate Bernstein–Greene–Krustal (BGK) solution. A BGK solution is considered to be adequate if it represents the nonlinear version of the natural eigenmodes of the plasma. Since the dust charge is allowed to change, we rewrite E_d as

$$E_d = \frac{1}{2} m_d v_d^2 + \chi = \frac{1}{2} m_d v_d^2 + \int_0^{\phi} q_d\, d\phi \tag{3}$$

so that E_d becomes a constant of the motion and thus $f(E_d)$ satisfies the stationary Vlasov equation. It is easy to show that

$$\frac{d\chi}{dx} = q_d \frac{d\phi}{dx}. \tag{4}$$

https://doi.org/10.1017/S0022377806004867 Published online by Cambridge University Press

We employ a vortex-like dust distribution function of Schamel [33] that solves the dust Vlasov equation. Thus, we have

$$f_{\rm d} = f_{\rm df} + f_{\rm dt} \tag{5}$$

with

$$f_{\rm df}(x, v_{\rm d}) = n_{\rm d0}\left(\frac{m_{\rm d}}{2\pi T_{\rm df}}\right)^{1/2} \times \exp\left(-\frac{m_{\rm d}v_{\rm d}^2/2 - e\int_0^\phi Z\, d\phi}{T_{\rm df}}\right) \quad \text{for } |v_{\rm d}| \succ \sqrt{\frac{2e\int_0^\phi Z\, d\phi}{m_{\rm d}}}, \tag{6}$$

$$f_{\rm dt}(x, v_{\rm d}) = n_{\rm d0}\left(\frac{m_{\rm d}}{2\pi T_{\rm df}}\right)^{1/2} \times \exp\left(-\beta_{\rm d}\frac{m_{\rm d}v_{\rm d}^2/2 - e\int_0^\phi Z\, d\phi}{T_{\rm df}}\right) \quad \text{for } |v_{\rm d}| \preceq \sqrt{\frac{2e\int_0^\phi Z\, d\phi}{m_{\rm d}}}, \tag{7}$$

where the subscript f (t) represents the free (trapped) dust contribution. Here $\beta_{\rm d}$ is a parameter determining the number of trapped dust grains and its magnitude is defined as the ratio of the free hot-dust temperature $T_{\rm df}$ to the hot trapped dust temperature $T_{\rm dt}$, i.e. $|\beta| = T_{\rm df}/T_{\rm dt}$. The introduction of the parameter $\beta_{\rm d}$ allows for a different temperature in the Maxwellian distribution for the trapped dust grains, $\beta_{\rm d} = 0$ ($\beta_{\rm d} = 1$) corresponding to a flat-topped (Maxwellian) dust distribution. Note that a hole in the trapped region, corresponding to an underpopulation of trapped dust particles, is represented by a negative $\beta_{\rm d}$ (a vortex-like excavated trapped dust distribution). It may be noted here that the distribution function (5) is continuous at the transition point between free and trapped particles and satisfies the regularity requirements for an admissible BGK solution. The slope of the trapped dust distribution function in velocity space is finite. With distribution (5) we obtain, for $\beta_{\rm d} < 0$,

$$n_{\rm d}(\phi) = \int_{-\infty}^{+\infty} f_{\rm d}(x, v_{\rm d})\, dv_{\rm d} = n_{\rm d0}\left\{\exp\left(-\frac{\chi}{T_{\rm df}}\right)\operatorname{erfc}\left(\sqrt{-\frac{\chi}{T_{\rm df}}}\right) + \frac{2}{\sqrt{-\pi\beta_{\rm d}}}W\left(\sqrt{\beta_{\rm d}\frac{\chi}{T_{\rm df}}}\right)\right\}. \tag{8}$$

Poisson's equation then becomes for $\beta_{\rm e}$, $\beta_{\rm d} < 0$,

$$\frac{d^2\Psi}{dX^2} = N_{\rm e} - fN_{\rm i} - \frac{(1-f)}{Q_{\rm d0}}Q_{\rm d}N_{\rm d} \tag{9}$$

where

$$N_{\rm e} = \frac{n_{\rm e}}{n_{\rm e0}} = \exp(\Psi)\operatorname{erfc}(\sqrt{\Psi}) + \frac{2}{\sqrt{-\pi\beta_{\rm e}}}W(\sqrt{-\beta_{\rm e}\Psi}), \tag{10}$$

$$N_{\rm i} = \frac{n_{\rm i}}{n_{\rm i0}} = \exp(-\sigma\Psi), \tag{11}$$

$$N_{\rm d} = \frac{n_{\rm d}}{n_{\rm d0}} = \exp(-\gamma\xi)\operatorname{erfc}(\sqrt{-\gamma\xi}) + \frac{2}{\sqrt{-\pi\beta_{\rm d}}}W(\sqrt{\beta_{\rm d}\gamma\xi}), \tag{12}$$

https://doi.org/10.1017/S0022377806004867 Published online by Cambridge University Press

and $f = n_{i0}/n_{e0}$, $\sigma = T_{ef}/T_i$, and $\gamma = rT_{ef}^2/e^2T_{df}$. The normalized quantities

$$\Psi = \frac{e\phi}{T_{ef}}, \quad \xi = \frac{e^2}{rT_{ef}^2}\chi, \quad X = \frac{x}{\lambda_{De}}, \quad Q_d = \frac{eq_d}{rT_{ef}}$$

are introduced and $\lambda_{De} = (T_{ef}/4\pi n_{e0}e^2)^{1/2}$ is the electron Debye length. Normalization of (4) yields

$$\frac{d\xi}{dX} = Q_d \frac{d\Psi}{dX}. \tag{13}$$

Charge neutrality at equilibrium requires $n_{e0} - n_{i0} + Z_0 n_{d0} = 0$. In the standard orbit-limited probe model for the dust grain [37], the latter is charged by the plasma currents at the grain surface. The charging current originates from electrons and ions hitting the grain surface. Accordingly, the variable dust charge $q_d = -eZ$ is determined self-consistently by (note that we consider a one-dimensional stationary plasma)

$$v_d \frac{dq_d}{dx} = I_e + I_i \tag{14}$$

where I_e and I_i are the average microscopic electron and ion currents entering the dust grains. The grain currents from the electrons and ions are [38–40]

$$I_j = \pi r^2 q_j (8T_j/\pi m_j)^{1/2} n_j W_j \tag{15}$$

where $r \ll \lambda_e$ is the grain radius and m_j are the masses. For $q_d < 0$, we have [41,42]

$$W_e = \exp(eq_d/rT_{ef}) \tag{16}$$

and

$$W_i = 1 - eq_d/rT_i. \tag{17}$$

We assume that the cold dust grains, whose mass is much greater than that of the ions, are accelerated by a weak presheath field to a velocity v_{d0}. Thus, the number conservation equation, after integration, yields

$$n_d v_d = n_{d0} v_{d0}. \tag{18}$$

After rearranging the terms in (14), one can obtain the following normalized charging equation,

$$\frac{dQ_d}{dX} = kN_d \left\{ -N_e \exp(Q_d) + \sqrt{\frac{\mu}{\sigma}} f N_i (1 - \sigma Q_d) \right\}, \tag{19}$$

with k given by

$$k = \sqrt{\frac{2n_{e0}e^2r^2}{m_e v_{d0}^2}} \tag{20}$$

and $\mu = m_e/m_i$. Equation (19) is the additional dynamical equation that is coupled to the plasma equations through the plasma currents. The dust electric charge becomes a dynamical variable that is coupled self-consistently to the other dynamical variables such as density and potential. Charge neutrality at equilibrium ($\Psi = 0$) requires the following constraint:

$$f = \sqrt{\frac{\sigma}{\mu}} \frac{\exp(Q_{d0})}{1 - \sigma Q_{d0}}. \tag{21}$$

https://doi.org/10.1017/S0022377806004867 Published online by Cambridge University Press

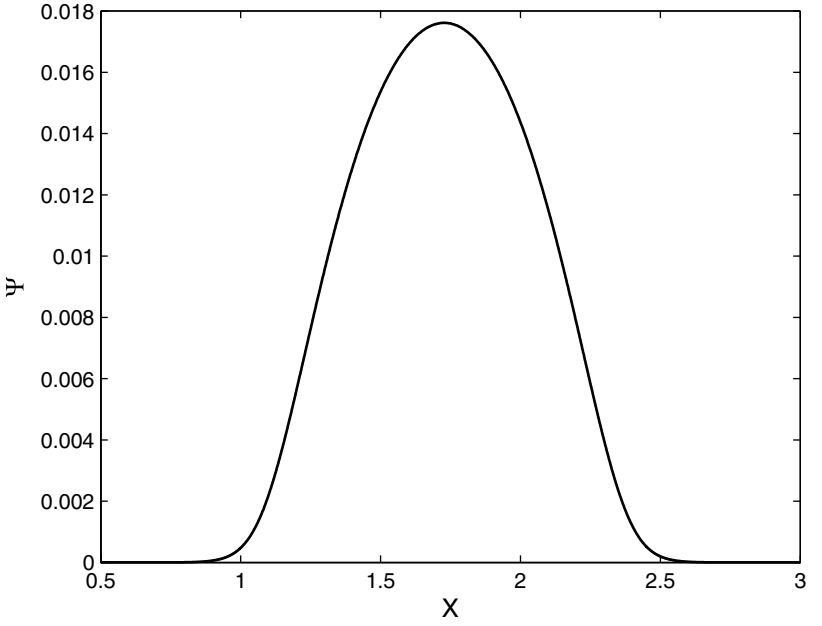


Figure 1. Soliton solution for the electrostatic potential Ψ with $Q_{\mathrm{d0}} = -1.56$, $T_{\mathrm{e}} = 1.5$ eV, $\sigma = 10$, $T_{\mathrm{df}} = T_{\mathrm{i}}/10$, $\beta_{\mathrm{d}} = -0.5$, $\beta_{\mathrm{e}} = -0.1$, $n_{\mathrm{i0}} = 10^8$ cm^{-3}, $v_{\mathrm{d0}} = 10^{-6}$ cm s^{-1}, and $r = 5 \times 10^{-3}$ μm. The value of $f = 1.71$ is deduced from (21).

In the following numerical simulation, the value of f is deduced from the above relation while the other remaining parameters ($Q_{\mathrm{d0}}, r, T_{\mathrm{ef}}, \sigma, T_{\mathrm{df}}, \beta_{\mathrm{e}}, \beta_{\mathrm{d}}, n_{\mathrm{i0}},$ and v_{d0}) are given first.

3. Numerical analysis and discussion

Equations (9), (13), and (19) are integrated numerically using a Runge–Kutta scheme suitable for stiff problems and assuming a hydrogen plasma. One can numerically solve the system of equations (9), (13), and (19) either as a boundary-value problem or as an initial-value problem. For simplicity, we have solved it as an initial value problem. To start the numerical integration, the initial value $\Psi(X = 0) = 0$ and a small edge electric field $E_0 = -(d\Psi/dX)(X = 0) = -10^{-12}$ are assumed. It is worth noting that one can take some other values of $(d\Psi/dX)$: an increase (decrease) in its value only shifts the potential or density profile towards (away from) the origin. We first consider the case when the grain charge remains constant and discuss later the case when the charge variations are self-consistently included. The electrostatic potential Ψ is given in Fig. 1, which exhibits a spatially localized (soliton-like) structure. The parameters $Q_{\mathrm{d0}} = -1.56$, $T_{\mathrm{ef}} = 1.5$ eV, $\sigma = 10$, $T_{\mathrm{df}} = T_{\mathrm{i}}/10$, $\beta_{\mathrm{d}} = -0.5$, $n_{\mathrm{i0}} = 10^8$ cm^{-3}, $\beta_{\mathrm{e}} = -0.1$, $v_{\mathrm{d0}} = 10^{-6}$ cm s^{-1}, and $r = 5 \times 10^{-3}$ μm ($r/\lambda_{\mathrm{De}} \sim 4.19 \times 10^{-6}$ and $r/\lambda_{\mathrm{Di}} \sim 1.73 \times 10^{-5}$) have been chosen. Figure 2 shows that when the charge of the dust grain is variable, the height as well as the width of the localized potential structure increase. The dust charge Q_{d} (Fig. 3) and the 'potential energy' ξ (Fig. 4) adopt the same localized profile as Ψ. Figure 5 indicates that the dust void (hole) increases when the grain charge variations are

https://doi.org/10.1017/S0022377806004867 Published online by Cambridge University Press

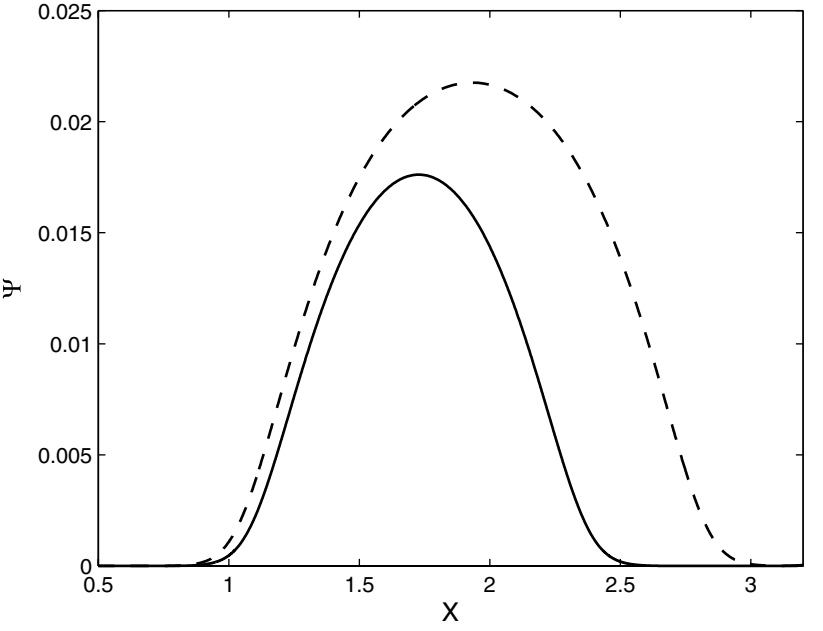


Figure 2. Soliton solution for the electrostatic potential Ψ. The values of the used parameters are the same as those used in Fig. 1. The solid line represents the case where the charge on the dust grain is constant and the dashed line represents the case where the charge on the dust grain is variable.

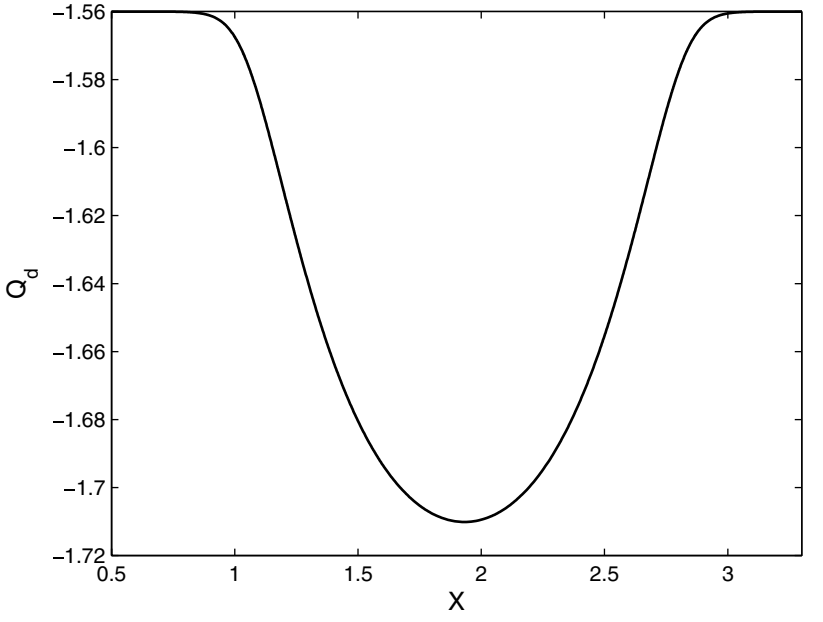


Figure 3. The spatial profile of dust grain charge Q_d. The values of the relevant parameters are the same as those used in Fig. 1.

https://doi.org/10.1017/S0022377806004867 Published online by Cambridge University Press

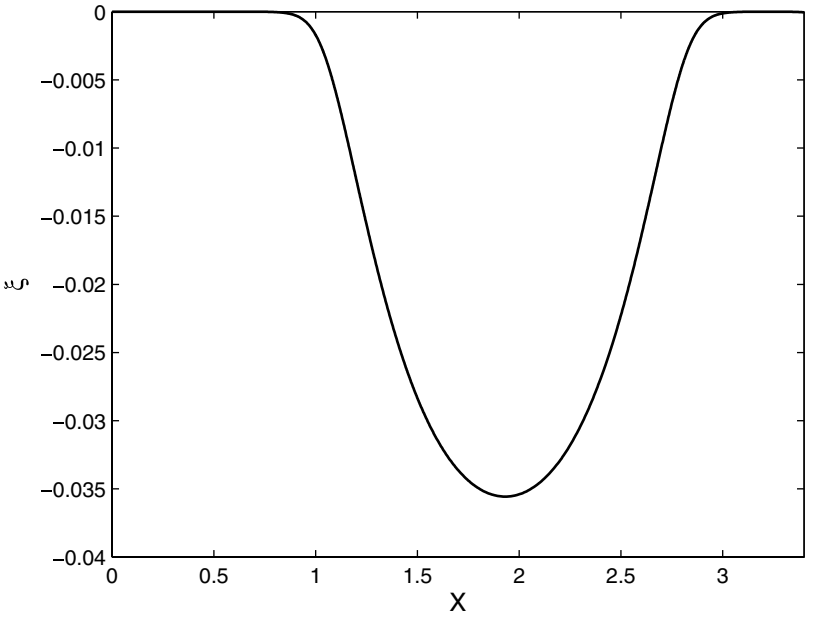


Figure 4. The spatial profile of dust grain 'potential energy' ξ. The values of the relevant parameters are the same as those used in Fig. 1.

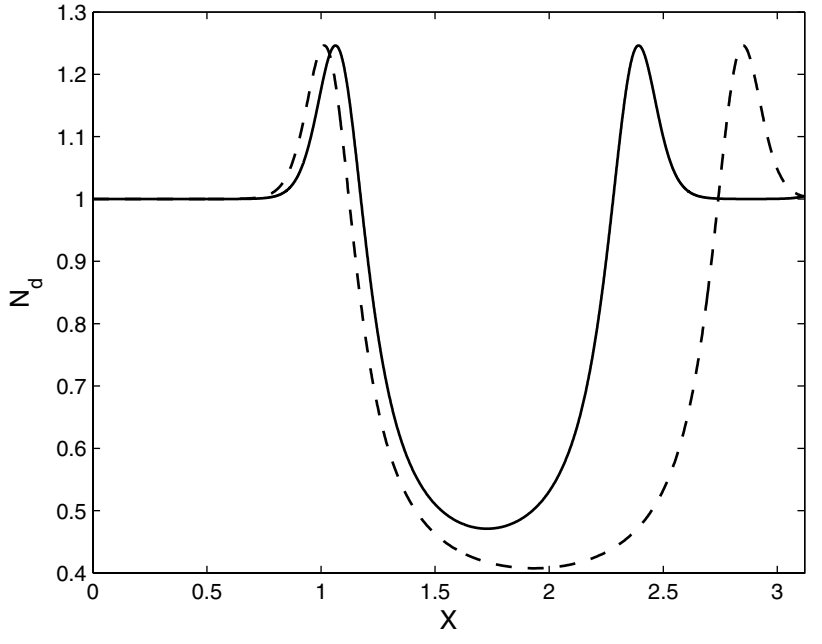


Figure 5. The spatial profile of dust density N_{d}. The values of the relevant parameters are the same as those used in Fig. 1. The solid line represents the case where the charge on the dust grain is constant and the dashed line represents the case where the charge on the dust grain is variable.

https://doi.org/10.1017/S0022377806004867 Published online by Cambridge University Press

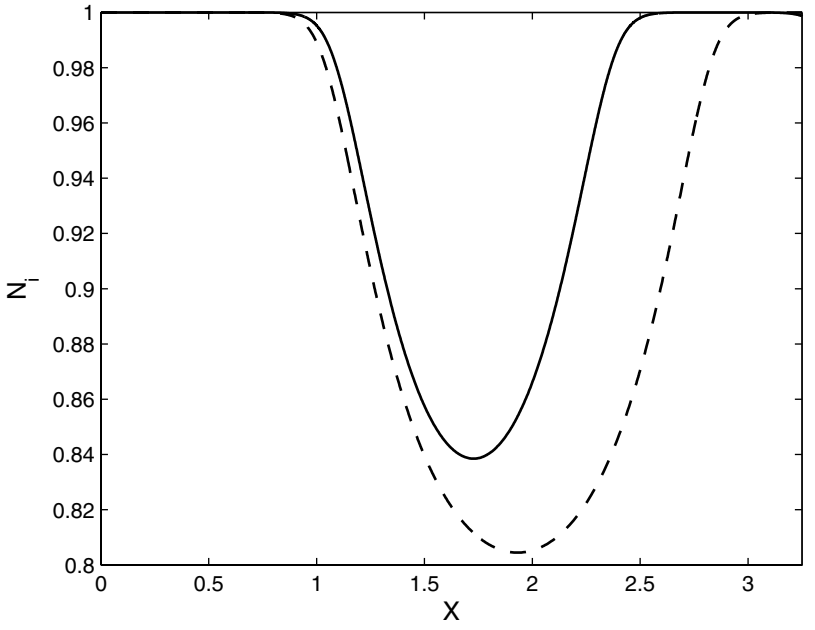


Figure 6. The spatial profile of the ion density N_i. The values of the relevant parameters are the same as those used in Fig. 1. The solid line represents the case where the charge on the dust grain is constant and the dashed line represents the case where the charge on the dust grain is variable.

accounted for (dashed line). The dust particles (Fig. 5) and the ions (Fig. 6) are locally expelled and pushed out of the region of the soliton's localization, a phenomenon that can generate an intense and spiky electric field in the medium. The electrons (Fig. 7) are found to be highly localized. This localization (accumulation) caused by a balance of the electrostatic forces acting on electrons is more effective in the case of variable dust charge. Consequently, the dust charge variation leads to an additional enlargement of the dust void (hole). This additional enlargement is less pronounced for smaller values of σ as can be seen on Fig. 8 ($\sigma = 4$) and more pronounced in the absence of resonant electrons (in the case of Boltzmann distributed electrons, $N_e = \exp(\Psi)$) (Fig. 9). It may be useful to note that we have carried out a numerical investigation over a wide range of plasma parameters and found that as the dust particle number density is increased, the depth, as well as the width, of the dust void decrease and the additional enlargement (due to dust charge perturbations) becomes less pronounced. The results compare favorably with what has been presented in [23, Fig. 2]. For the sake of comparison, we have plotted the dust number density profiles for various values of $\sigma = T_{ef}/T_i$ (Fig. 10) and $|\beta_d| = T_{df}/T_{dt}$ (Fig. 11). Figure 10 (Fig. 11) implies that the dust voids shrink (enlarge) when σ ($|\beta_d|$) is decreased. Figure 12 (Fig. 13) indicates that the dust charge becomes less (more) negative as σ ($|\beta_d|$) is decreased. Figure 14 shows that as we increase $|\beta_e|$, the depth, as well as the width, of the dust void decrease. Furthermore, it is interesting to note that the additional enlargement (due to dust charge perturbations) becomes slightly less pronounced at larger values of $|\beta_e|$ (Figs 15 and 16). Consequently, the dust voids shrink when the electrons deviate from isothermality.

https://doi.org/10.1017/S0022377806004867 Published online by Cambridge University Press

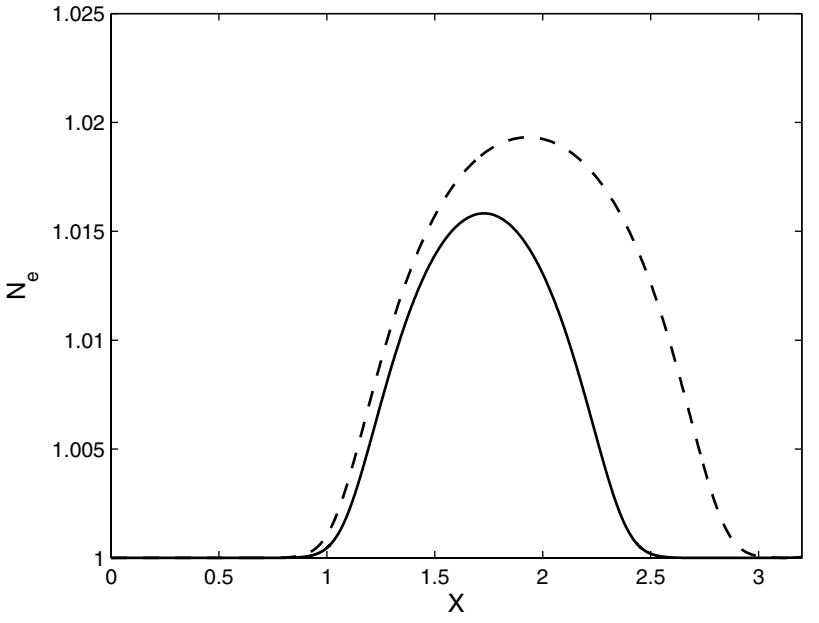


Figure 7. The spatial profile of the electron density N_e. The values of the relevant parameters are the same as those used in Fig. 1. The solid line represents the case where the charge on the dust grain is constant and the dashed line represents the case where the charge on the dust grain is variable.

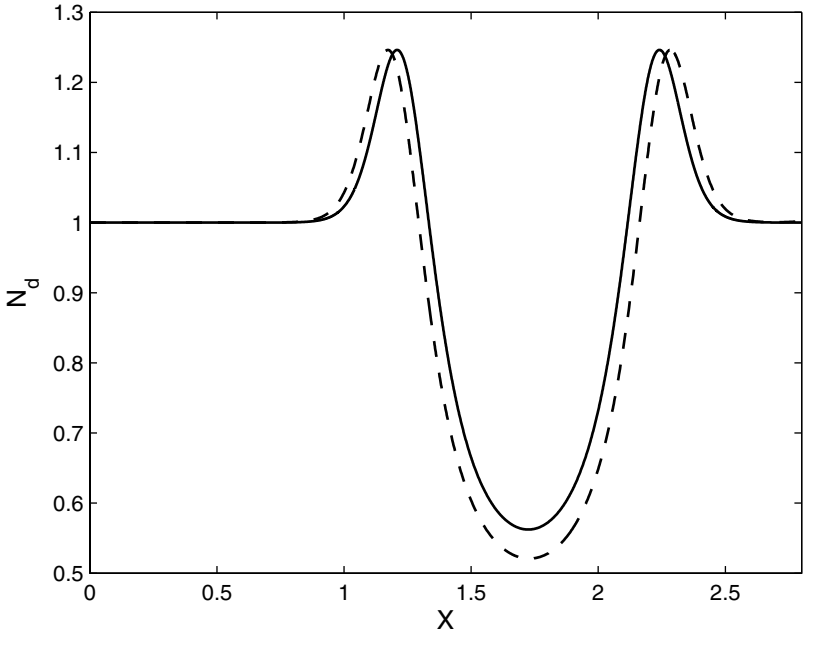


Figure 8. The spatial profile of the dust density N_d. The values of the relevant parameters are the same as those used in Fig. 1 with $\sigma = 4$. The solid line represents the case where the charge on the dust grain is constant and the dashed line represents the case where the charge on the dust grain is variable. The value of $f = 2.48$ is deduced from (21).

https://doi.org/10.1017/S0022377806004867 Published online by Cambridge University Press

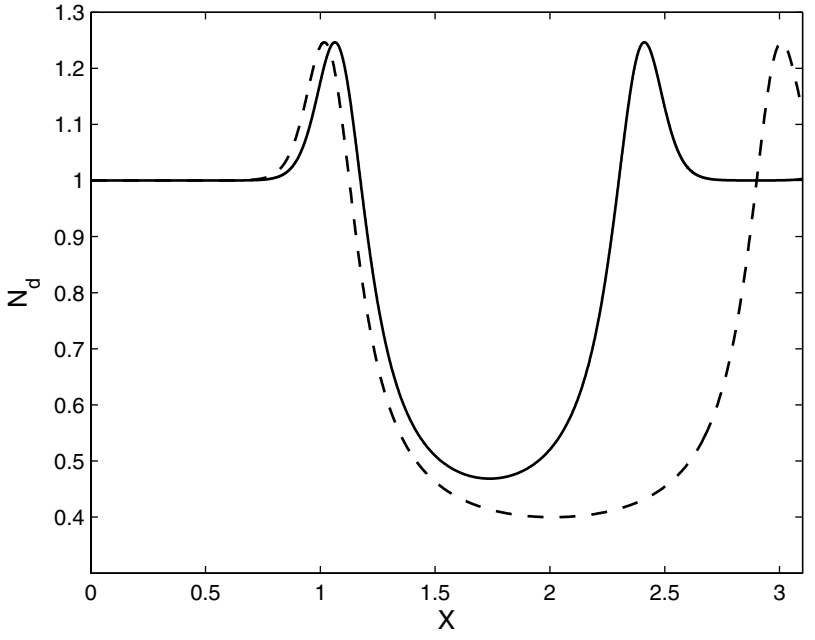


Figure 9. The spatial profile of the dust density N_d. The values of the relevant parameters are the same as those used in Fig. 1 with Boltzmann distributed electrons. The solid line represents the case where the charge on the dust grain is constant and the dashed line represents the case where the charge on the dust grain is variable.

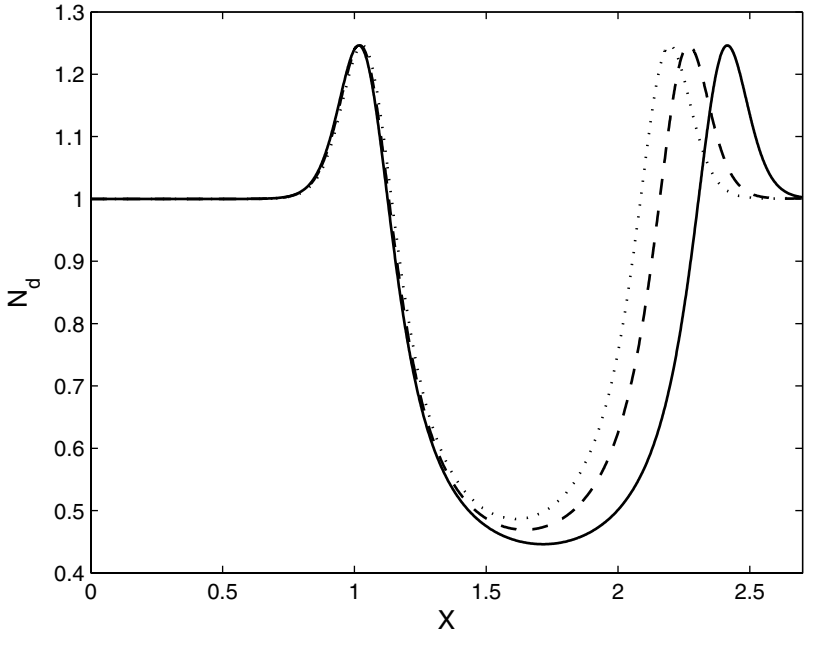


Figure 10. The spatial profile of the dust density N_d in the case of variable charge for different values of $\sigma = 9$ (solid line, $f = 1.79$), $\sigma = 8$ (dashed line, $f = 1.88$), and $\sigma = 7$ (dotted line, $f = 1.99$). The values of the remaining parameters are the same as those used in Fig. 1.

https://doi.org/10.1017/S0022377806004867 Published online by Cambridge University Press

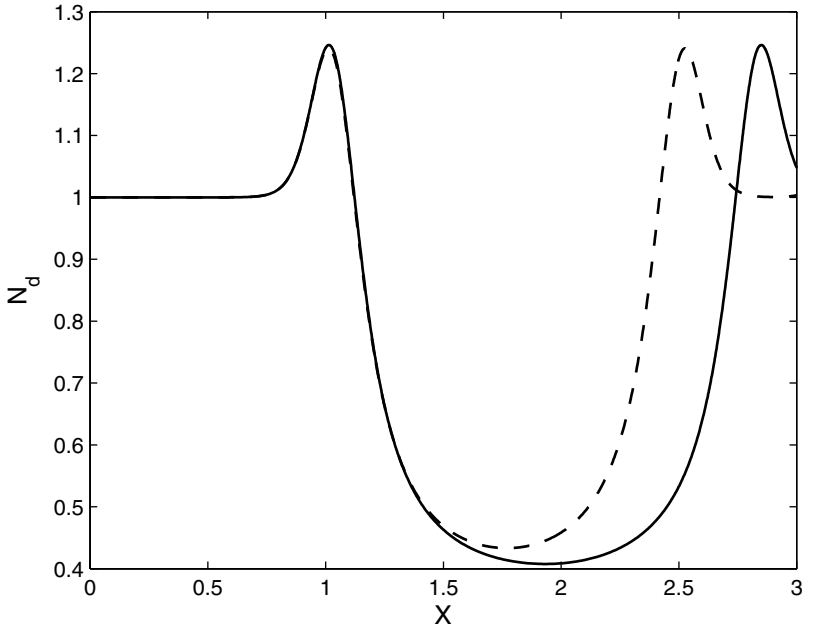


Figure 11. The spatial profile of the dust density $N_{\rm d}$ in the case of variable charge for two different values of $\beta_{\rm d} = -0.5$ (solid line) and $\beta_{\rm d} = -0.51$ (dashed line). The values of the remaining parameters are the same as those used in Fig. 1.

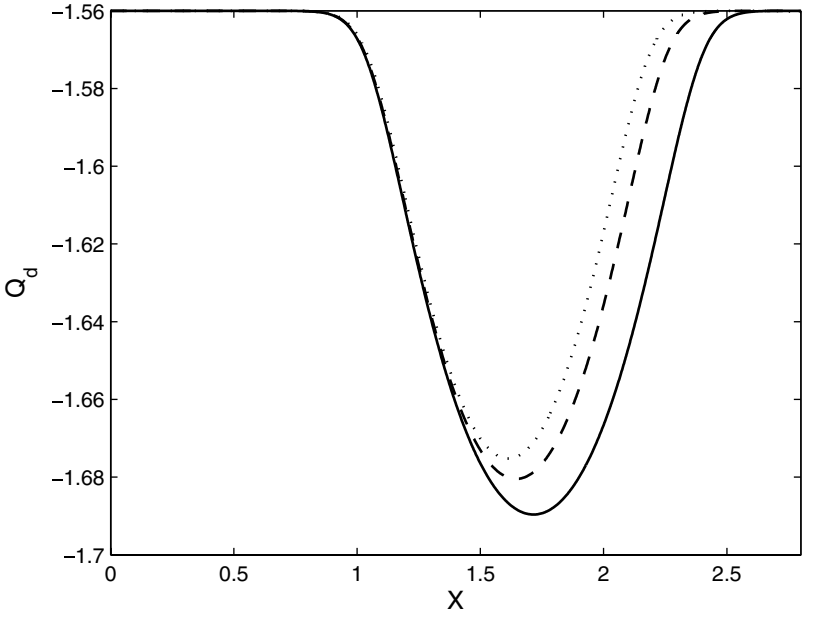


Figure 12. The spatial profile of the dust grain charge $Q_{\rm d}$ for different values of $\sigma = 9$ (solid line, $f = 1.79$), $\sigma = 8$ (dashed line, $f = 1.88$), and $\sigma = 7$ (dotted line, $f = 1.99$). The values of the remaining parameters are the same as those used in Fig. 1.

https://doi.org/10.1017/S0022377806004867 Published online by Cambridge University Press

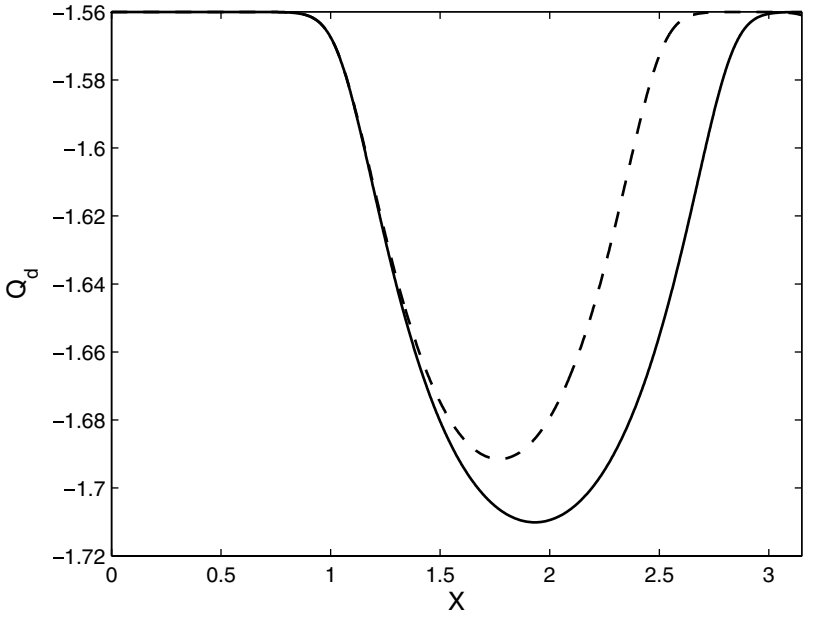


Figure 13. The spatial profile of the dust grain charge Q_d for two different values of $\beta_d = -0.5$ (solid line) and $\beta_d = -0.51$ (dashed line). The values of the remaining parameters are the same as those used in Fig. 1.

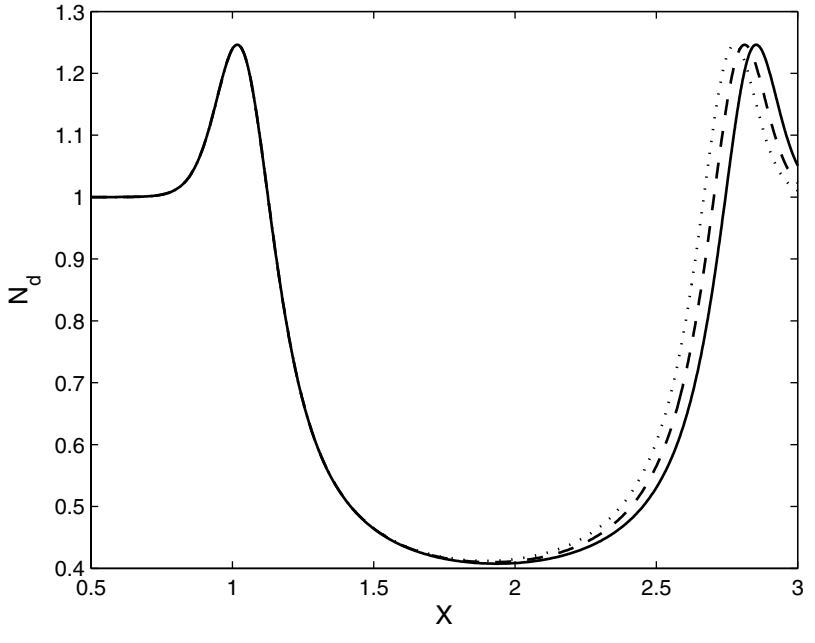


Figure 14. The spatial profile of the dust density N_d in the case of variable charge for different values of $\beta_e = -0.1$ (solid line), $\beta_d = -0.5$ (dashed line), and $\beta_d = -0.9$ (dotted line). The values of the remaining parameters are the same as those used in Fig. 1.

https://doi.org/10.1017/S0022377806004867 Published online by Cambridge University Press

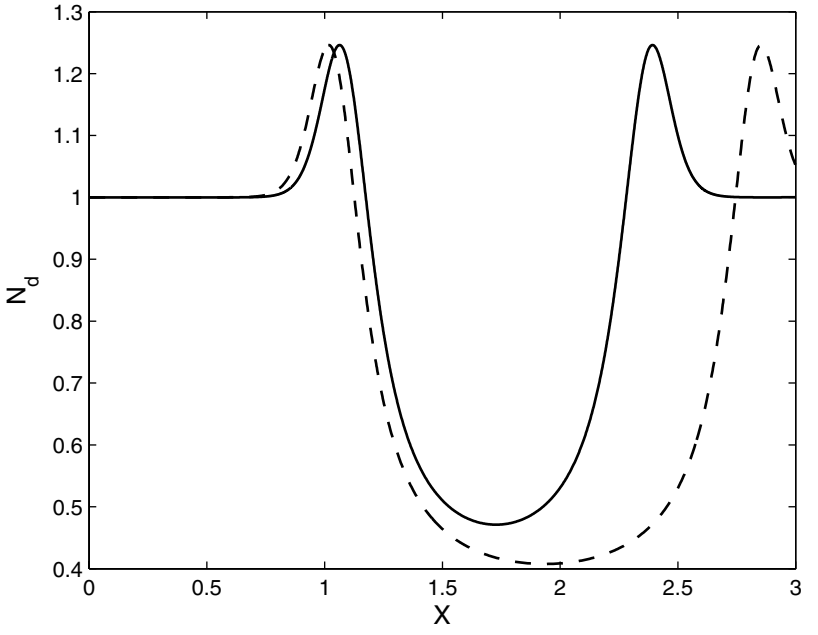


Figure 15. The spatial profile of the dust density N_d. The values of the relevant parameters are the same as those used in Fig. 1 with $\beta_e = -0.1$. The solid line represents the case where the charge on the dust grain is constant and the dashed line represents the case where the charge on the dust grain is variable.

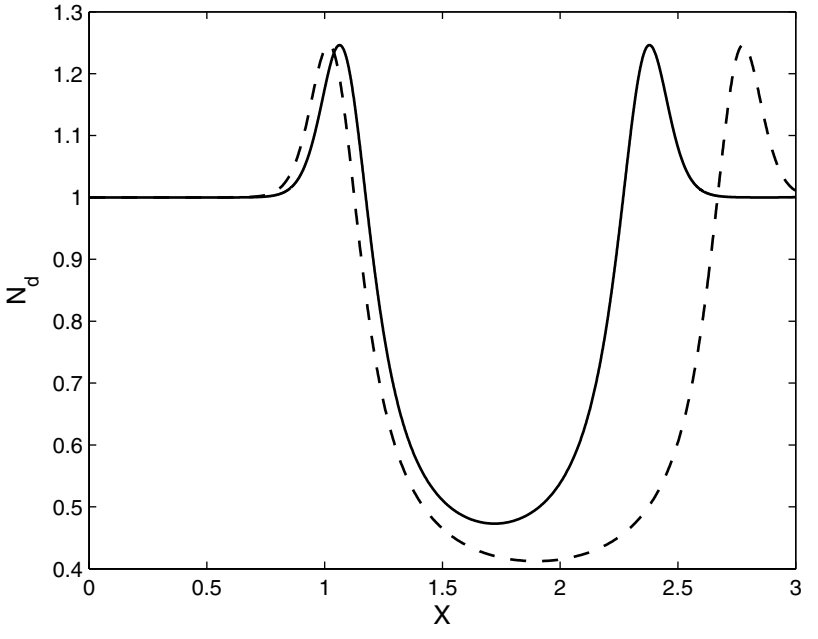


Figure 16. The spatial profile of the dust density N_d. The values of the relevant parameters are the same as those used in Fig. 1 with $\beta_e = -0.9$. The solid line represents the case where the charge on the dust grain is constant and the dashed line represents the case where the charge on the dust grain is variable.

https://doi.org/10.1017/S0022377806004867 Published online by Cambridge University Press

4. Conclusion

In conclusion, we have extended the recent analysis of dust voids [32] to include the dust charge variation and electron trapping, and thereby shown that under certain conditions the effect of dust charge variation can be quite important and can lead to a significant departure from the behavior reported in [32]. In particular, it may be noted that the dust charge variation leads to an additional enlargement of these nonlinear dust voids. As the dust particle number density is increased, the depth, as well as the width, of the dust void decrease and the additional enlargement (due to dust charge perturbations) becomes less pronounced. The dust voids exhibit smaller widths than those involving isothermal electrons. At present, we do not have any experimental observations of dust voids (holes) in dusty plasmas with variable charge to compare with our theoretical predictions. However, considering the wide relevance of nonlinear oscillations in laboratory and space dusty plasmas, our investigation may be taken as a prerequisite for the understanding of the large, but finite-amplitude, solitary waves that may occur in space and laboratory plasmas. It may be stressed here that the time evolution and stability analysis of these nonlinear dust voids (holes) are problems of great importance but beyond the scope of the present work.

Acknowledgement

This work was supported in part by the Ministère de l'Enseignement Supérieur et de la Recherche Scientifique Contract No. D1602/04/03.

References

[1] Goertz, C. K. 1989 *Rev. Geophys.* **27**, 271.
[2] Mendis, D. A. and Rosenberg, M. 1994 *Ann. Rev. Astron. Astrophys.* **32**, 419.
[3] Horanyi, M. 1996 *Ann. Rev. Astron. Astrophys.* **34**, 383.
[4] Verheest, F. 2000 *Waves in Dusty Space Plasmas*. Dordrecht: Kluwer.
[5] Shukla, P. K. and Mamun, A. A. 2002 *Introduction to Dusty Plasma Physics*. Bristol: Institute of Physics.
[6] Rao, N. N., Shukla, P. K. and Yu, M. Y. 1990 *Planet. Space Sci.* **38**, 543.
[7] Shukla, P. K. and Silin, V. P. 1992 *Phys. Scr.* **45**, 508.
[8] Tribeche, M. and Zerguini, T. H. 2001 *Phys. Plasmas* **8**, 394.
[9] Tribeche, M., Houili, H. and Zerguini, T. H. 2002 *Phys. Plasmas* **9**, 419.
[10] Tribeche, M. and Zerguini, T. H. 2004 *Phys. Plasmas* **11**, 4115.
[11] Melzer, A., Homann, A., Piel, A., Schweigert, V. A. and Schweigert, I. V. 1998 *Physics of Dusty Plasmas (AIP Conf. Proc., 446)*. Woodbury: AIP, p. 167.
[12] Samsonov, D. and Goree, J. 1999 *Phys. Rev.* E **59**, 1047.
[13] Praburam, G. and Goree, J. 1996 *Phys. Plasmas* **3**, 1212.
[14] Goree, J., Morfill, G. E., Tsytovich, V. N. and Vladimirov, S. V. 1999 *Phys. Rev.* E **59**, 7055.
[15] Morfill, G. E., Thomas, H. M., Konopka U., Rothermel, H., Zuzic, M., Ivlev, A. and Goree, J. 1999 *Phys. Rev. Lett.* **83**, 1598.
[16] Tsytovich, V. N., Vladimirov, S. V., Morfill, G. E. and Goree, J. 2001 *Phys. Rev.* E **63**, 056609.
[17] Avinash, K. 2001 *Phys. Plasmas* **8**, 2601.
[18] Tsytovich, V. N. 2001 *Phys. Scr.* **T89**, 89.

https://doi.org/10.1017/S0022377806004867 Published online by Cambridge University Press

[19] Khrapak, S. A., Ivlev, A. V., Morfill, G. E. and Thomas, H. M. 2002 *Phys. Rev.* E **66**, 046414.

[20] Zafiu, C., Melzer, A. and Piel, A. 2002 *Phys. Plasmas* **9**, 4794.

[21] Zafiu, C., Melzer, A. and Piel, A. 2003 *Phys. Plasmas* **10**, 1278.

[22] Khrapak, S. A., Ivlev, A. V., Morfill G. E. and Thomas, H. M. 2003 *Phys. Plasmas* **10**, 4579.

[23] Mamun, A. A., Shukla, P. K. and Bingham, R. 2002 *Phys. Lett.* A **298**, 179.

[24] Dahiya, R. P., Paeva, G. V., Stoffels, W. W., Stoffels, E., Kroesen, G. M. W., Avinash, K. and Bhattacharjee, A. 2002 *Phys. Rev. Lett.* **89**, 125001.

[25] Avinash, K., Bhattacharjee, A. and Hu, S. 2003 *Phys. Rev. Lett.* **90**, 075001.

[26] Jovanović, D. and Shukla, P. K. 2003 *Phys. Lett.* A **308**, 369.

[27] Jovanovic, J. and Shukla, P. K. 2004 *Phys. Scr.* **T107**, 188.

[28] Mikikian, M. and Boufendi, L. 2004 *Phys. Plasmas* **11**, 3733.

[29] Mamun, A. A. and Shukla, P. K. 2004 *Phys. Plasmas* **11**, 1757.

[30] Tribeche, M., Aoutou, K. and Zerguini, T. H. 2005 *Phys. Plasmas* **12**, 032305.

[31] Tribeche, M., Ait Gougam, L., Aoutou, K. and Zerguini, T. H. 2005 *Phys. Plasmas* **12**, 092309.

[32] Mamun, A. A. and Shukla, P. K. 2005 *J. Plasma Phys* **71**, 143.

[33] Schamel, H. 1986 *Phys. Reports* **140**, 161.

[34] Schamel, H. and Bujarbarua, S. 1980 *Phys. Fluids* **23**, 2498.

[35] Schamel, H. 2000 *Phys. Plasmas* **7**, 4831.

[36] Schamel, H., Das, N. and Rao, N. N. 2001 *Phys. Plasmas* **8**, 671.

[37] Chen, F. F. 1965 *Plasma Diagnostic Techniques* (ed. R. H. Huddlestone and S. L. Leonard). New York: Academic Press, ch. 4.

[38] Barnes, M. S., Keller, J. H., Forster, J. C., O'Neill, J. A. and Coultas, D. K. 1992 *Phys. Rev. Lett.* **68**, 313.

[39] Ma, J. X. and Yu, M. Y. 1995 *Phys. Plasmas* **2**, 1343.

[40] Whipple, E. C. 1981 *Rep. Prog. Phys.* **44**, 1198.

[41] Ma, J. X., Liu, J.-y. and Yu, M. Y. 1997 *Phys. Rev.* E **55**, 4627.

[42] Liu, J.-y. and Ma, J. X. 1997 *Phys. Plasmas* **4**, 2798.

https://doi.org/10.1017/S0022377806004867 Published online by Cambridge University Press